

Preprocessing-based Kinodynamic Motion Planning Framework for Intercepting Projectiles using a Robot Manipulator

Ramkumar Natarajan¹, Hanlan Yang¹, Qintong Xie², Yash Oza¹, Manash Pratim Das¹, Fahad Islam¹, Muhammad Suhail Saleem¹, Howie Choset¹, and Maxim Likhachev¹

Abstract—We are interested in studying sports with robots and starting with the problem of intercepting a projectile moving toward a robot manipulator equipped with a shield. To successfully perform this task, the robot needs to (i) detect the incoming projectile, (ii) predict the projectile’s future motion, (iii) plan a minimum-time rapid trajectory that can evade obstacles and intercept the projectile, and (iv) execute the planned trajectory. These four steps must be performed under the manipulator’s dynamic limits and extreme time constraints ($\leq 350\text{ms}$ in our setting) to successfully intercept the projectile. In addition, we want these trajectories to be smooth to reduce the robot’s joint torques and the impulse on the platform on which it is mounted. To this end, we propose a kinodynamic motion planning framework that preprocesses smooth trajectories offline to allow real-time collision-free executions online. We present an end-to-end pipeline along with our planning framework, including perception, prediction, and execution modules. We evaluate our framework experimentally in simulation and show that it has a higher blocking success rate than the baselines. Further, we deploy our pipeline on a robotic system comprising an industrial arm (ABB IRB-1600) and an onboard stereo camera (ZED 2i), which achieves a 78% success rate in projectile interceptions.

I. INTRODUCTION

In this paper, we study the problem of intercepting incoming projectiles using robotic manipulators through the application of kinodynamic planning. This is a challenge that finds unique and thrilling applications in various sports. Recent breakthroughs in this field include instances where robots have coped with diverse spin types in table tennis matches against human opponents [1] and instances where robots have skillfully intercepted flying, rolling, and bouncing balls [2]. These scenarios represent the exciting intersection of sports and robotics. In our problem, our primary goal is to efficiently intercept incoming projectiles with robotic manipulators. We aim to demonstrate how robotic systems, equipped with kinodynamic planning capabilities, can plan smooth trajectories while minimizing torque requirements.

The time-critical nature of the task calls for an intelligent framework that can maximize the robot’s chances of intercepting projectiles. Based on the range of the vision system and average velocities of the incoming projectiles in our setting, the robot typically has about 350 milliseconds from when the projectile is first detected until it hits the body of the robot. Within this time frame, our framework should be capable of performing three major tasks: (i) detecting and

accurately predicting the motion of the incoming projectile, (ii) querying a motion planner for a manipulator trajectory that would enable the robot to safely intercept the projectile, and (iii) executing the trajectory returned by the motion planner in the real world. The fast nature of the task, combined with the physical limitations of the robot (typical executions of blocking maneuvers consume about 250 of the 350 milliseconds available to us), calls for a realtime yet optimal planning framework. In this manuscript, we present our pipeline that comprises (i) an on-board stereo camera-based perception module that provides estimates of the incoming projectile and its predicted trajectory and (ii) a preprocessing-based planning framework that guarantees to return a blocking trajectory if it exists (based on the perception estimates) within a significantly small time budget (1ms).

The contributions of our work can be summarized as follows:

- The formulation of the problem of robot protection against incoming projectiles and the development of the framework consisting of real-time perception, motion planning, and execution.
- A preprocessing-based motion planning module that guarantees to return blocking trajectories within an extremely small time window.
- A *dome-based* discretization technique that makes preprocessing tractable while still providing strong guarantees.
- Demonstration of the effectiveness of our pipeline in the real world by deploying it on an ABB’s IRB-1600 robot arm and a ZED 2i stereo camera setup, as shown in Fig. 1.

II. RELATED WORK

There are several works in the literature that have investigated tasks that are similar to the task of intercepting projectiles. In this section, we will discuss these works, as well as their advantages and disadvantages. In [3], the authors presented a framework that can be utilized by robot manipulators to catch a ball. Specifically, the catching problem is formulated as a bi-level optimization problem, which produces a joint trajectory that can successfully complete the catching task. The advantage of using an optimization-based trajectory generation algorithm is that trajectories can be quickly generated in simple environments even for high-dimensional planning problems. There are three key disadvantages in this work as compared to our work: (i) as [3] solves an optimization problem online while the projectile

¹The Robotics Institute, School of Computer Science, Carnegie Mellon University, USA. {rnataraj, hanlany, yoza, mpratimd, fi, choset, mlikhach}@andrew.cmu.edu

²Department of Engineering Science, University of Oxford, UK. qintong.xie@univ.ox.ac.uk

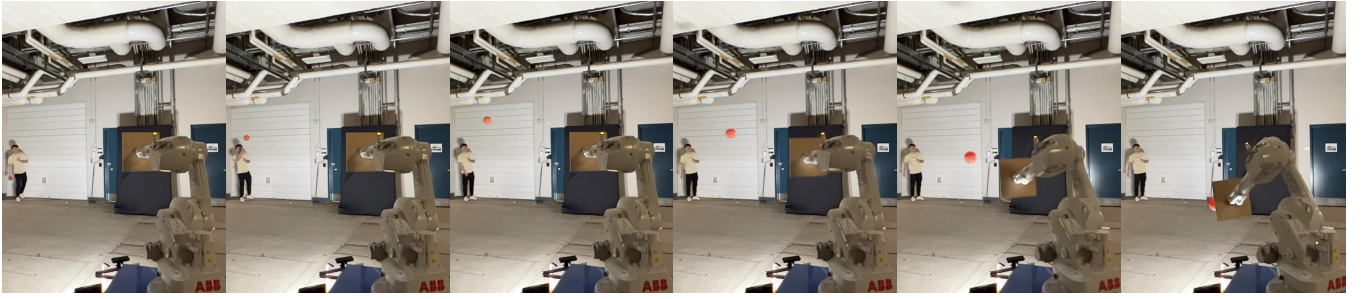


Fig. 1. ABB arm with a shield attached to its end-effector blocking a ball thrown at it.

is in flight, it is not guaranteed to return a solution within a strict time limit; (ii) [3] assumes that there are no obstacles in the workspace; (iii) [3] uses a VICON system that provides very accurate pose estimate of the incoming object. Hence, the assumptions of the planning and the perception problems in [3] are stronger than the ones in our framework. Since our pipeline avoids obstacles, performs object pose estimation and re-estimation using RGB-D sensors, and does not assume a motion capture system. [4] and [5] use reinforcement learning in a model-free setting to learn policies that are capable of generating dynamic strokes for the table-tennis playing robot. The main advantage of using machine learning-based methods is that the policies learnt by the neural network can generalize to new data points that are similar to previously seen data points. However, these approaches require training a large set of data, especially if the scenes are allowed to have obstacles [6].

On the perception side, RGB-D cameras are very noisy and thus require special filtering techniques to detect incoming projectile. Model specific methods like [7] attempts to fit a known 3D model to the point cloud to efficiently find the location of the projectile. However, this assumes that the model of the projectile is known. There also exist more generic approaches like [8] does not have such requirements. But these methods either require a laser scanner or a VICON system [9] to detect the moving object. Recently, machine learning-based methods have also gained popularity for object detection [10]. For example, YOLO [11] can be utilized for object detection and tracking. However, it cannot detect the fast-moving ball at a distance. Hence, this method requires substantial data for training, making it challenging to predict their performance on new data points. In our work, we employ a straightforward color detection algorithm to detect the projectile using a single stereo camera. This approach enhances the practicality of our framework in real-world scenarios.

III. PROBLEM FORMULATION

Consider a robot manipulator with a shield rigidly attached to the end-effector of the manipulator. The manipulator is tasked with protecting a specific object. A projectile is launched in the direction of the object to be protected, and the manipulator must intercept the projectile before it collides with that object. The state of the projectile, ρ , is represented as a tuple (ρ_p, ρ_v) , where $\rho_p \in \mathbb{R}^3$ represents the position, and $\rho_v \in \mathbb{R}^3$ represents the velocity of the projectile. The

goal of the problem is to intercept the projectile before it collides with the object which is to be protected \mathcal{O} . To solve this problem, we make certain simplifying assumptions:

- The manipulator always starts from a “home” configuration s_{home} .
- The projectile is launched from within the field of view of the camera, allowing us to get early estimates of its trajectory ρ .
- At any point in time, only a single projectile is launched in the direction of \mathcal{O} .

Let \mathcal{T}_t be the time of flight of the projectile, measured from the time it is first observed to when it collides with \mathcal{O} . Let \mathcal{T}_d be the time duration for the perception module to collect enough frames and finish estimating the trajectory. Finally, let \mathcal{T}_p be the time taken to query the motion planner for a manipulator trajectory, and \mathcal{T}_e be the time taken by the manipulator to execute that trajectory.

In order for the manipulator to successfully intercept the projectile, two conditions need to be satisfied. First, given a long enough time-out, a motion planner must be able to compute a trajectory from s_{home} to a goal configuration which can intercept the projectile. Second, the manipulator also needs to ensure that it reaches the goal configuration before the projectile passes that location (in \mathbb{R}^3). Specifically, the following equation needs to be satisfied:

$$\mathcal{T}_t \geq \mathcal{T}_d + \mathcal{T}_p + \mathcal{T}_e \quad (1)$$

IV. METHOD

A. System Overview

The constraints laid out by the problem call for deriving an approach that minimizes time spent on any online operation, hence budgeting as much time as possible for execution and perception. To this end, we propose an approach relies heavily on pre-computation, similar to the Constant-Time Motion Planning (CTMP) class of algorithms [12].

At a high level, each camera-captured frame is processed within the perception module shown in Figure 2. Once a sufficient number of frames meeting the specified criteria are detected, these frames, together with their respective timestamps, are used to estimate the trajectory of the projectile. The derived positions and velocities of the projectile are then published to the planner. Subsequently, through an offline solution of a series of planning problems and the storage of their outcomes in a database, we can query and obtain a path for the manipulator’s trajectory. During execution, this

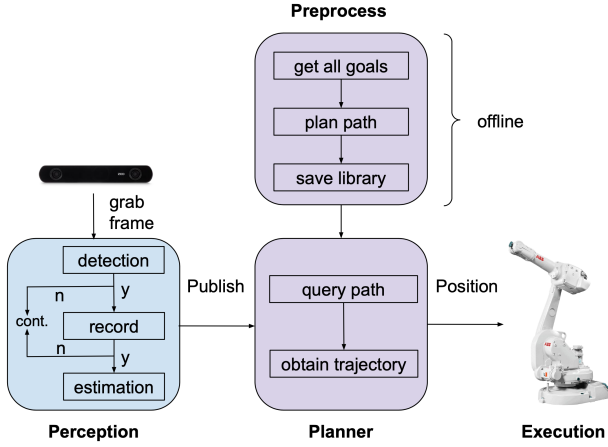


Fig. 2. Flowchart showing the overall pipeline.

trajectory is executed to intercept the projectile and prevent any potential collisions with object \mathcal{O} . In the remainder of the section, we discuss the proposed approach and its building blocks in detail (Section IV-B and IV-C), and provide the complete algorithm (Section IV-D, IV-E, IV-E.1, and IV-F).

B. Proposed Approach

In our approach, we define two cuboidal *domes* around the object \mathcal{O} , an inner dome D_i and an outer dome D_o . D_i approximates the geometry of the object \mathcal{O} and D_o captures the robot's reachable space so that it can intercept the projectiles with the shield \mathcal{S} positioned anywhere in the 3D space between D_i and D_o . The two domes are discretized into cells. Our planning approach is divided into two stages - the preprocessing stage and the query stage. In the preprocessing stage, for each pair of cells (with one cell from D_i and one cell from D_o), we plan a path to a pose of \mathcal{S} that can block all projectiles passing through the pair of cells. These paths are stored in a lookup table mapping the pair of cells to the corresponding path. In the query stage, for an incoming projectile ρ , we first identify the pair of cells through which ρ passes. Second, we look up the corresponding path π from the look up table in constant time. For replanning, additional paths are pre-computed from the states on these paths. This process runs recursively as newly computed paths create new replannable states which also must be processed.

With this approach, the size of the goal region \mathcal{G} becomes equal to the total number of pairs of cells. Note that these cells are computed only with two-dimensional discretization of the domes' surfaces as opposed to six-dimensional discretization of the space of projectiles. This greatly reduces the size of \mathcal{G} .

C. Proposed Approach Building Blocks

1) *Domes Specification*: The geometry of D_i is such that it tightly encapsulates the object \mathcal{O} , or in other words over approximates the geometry of \mathcal{O} with a simple shape. With this, we simplify the problem setup by making a more

conservative requirement that D_i must be protected instead of \mathcal{O} . We define D_i as a cuboid.

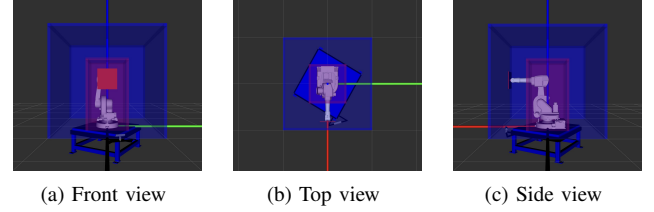


Fig. 3. (a) and (b) show the inner (red) and outer (blue) domes surrounding the robot. (c) shows the ABB's robot arm with a shield attached to its end-effector (in simulation).

The outer dome D_o captures the reachable workspace of the robot. For simplicity, we also define D_o as a cuboid. We keep D_o co-centric with D_i but it is larger than D_i . A larger D_o would allow more freedom to the robot but would also increase the preprocessing demand. On the other hand, a smaller D_o would restrict the robot and limit its protection capability. We choose the size of D_o such that the manipulator can reach the side it faces at full extension. While our approach is simple, it can be readily generalized to different robot models. Figure 3 shows the two domes configured for the ABB's robot arm. The volume between the D_o and D_i is where the robot manipulates the shield to intercept incoming projectiles.

2) *Domes Discretization and Shield Geometry*: Each side of D_i and D_o are discretized into cells. The discretization is correlated with the shape and size of \mathcal{S} . We use a square-shaped \mathcal{S} of in our setup. The discretization of the two domes is shown in Figure 4 (a). It is also to be noted that the size of the shield in our application can be made significantly large in order to decrease the preprocessing effort. But doing this is not always practical, and could violate the task and environment constraints.

The protrusion of each pair of cells (with one cell from D_i and one cell from D_o) along a straight line into the volume between D_o and D_i constitutes a *tunnel*. A line segment connecting the centers of the cells forming the tunnel is called *centerline*. Our key idea is that if \mathcal{S} is positioned such that it fully blocks this tunnel, all possible attacks that cross the pair of cells are blocked by it. This idea is illustrated in Figure 4 (b).

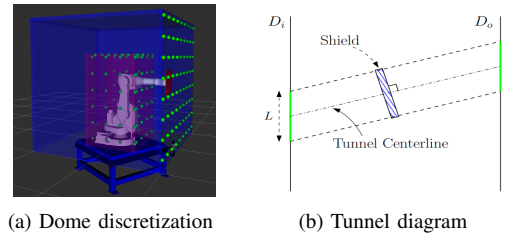


Fig. 4. (a) shows the centers of the cells on both domes. For D_o we only show the discretization for the front side. (b) shows a tunnel formed by a pair of cells (shown in green) in D_o and D_i .

The size of the cells is proportional to the size of \mathcal{S} . Specifically, we choose the cell size to be smaller than the size of \mathcal{S} to allow some tolerance for the pose of \mathcal{S} that blocks the tunnel. This tolerance is needed for possible

planning and execution errors. We performed a thorough geometric analysis of the magnitude of reduction in cell size that is needed to account for these errors. The related derivations and equations have been left out for brevity.

We approximate the portion of the projectile that lies between the two domes by a line segment. This approximation is made under the assumption that the objects move in a straight line within that region and therefore do not breach the boundaries of the tunnel which they enter. This is not too strong of an assumption if the distance between D_i and D_o is small compared to the distance from which the attacks are launched. This assumption can be lifted by performing an analysis for the reduction in cell size needed to account for the projectile to line segment approximate error. We leave this analysis for future work.

3) *Goal Condition*: The goal $g \in \mathcal{G}$ is defined as the centerline of a tunnel. For the motion planner, the goal condition is any pose of S along the centerline, such that S is oriented orthogonal to it (see Figure 4 (b)). For ease of planning, we allow small tolerance in $SE(3)$ for the goal pose. In our implementation, we sample equidistant points along the tunnel's centerline and compute $SE(3)$ poses at each point which are orthogonal to it. The motion planner then attempts to plan to each of these poses sequentially, until it succeeds. If it fails to do so, then the corresponding \mathcal{G} is marked as unreachable.

4) *Motion Planner*: We use a heuristic search-based planning approach with motion primitives (see, e.g. [13], [14], [15]) as they have strong optimality guarantees. The states and the transitions implicitly define a graph $G = (S, E)$ where S is the set of all states and E is the set of all transitions defined by the motion primitives. We use a kinodynamic planning algorithm INSAT, which is explained in details in IV-E.

D. Offline Preprocessing and Online Querying

1) *Preprocessing Stage*: In the preprocessing stage, for each pair of cells, the tunnel centerlines are computed. Each tunnel is checked for feasibility. Namely, the tunnels whose volume snaps to zero anywhere along the length are discarded because no incoming object coming through such a tunnel can reach the tunnel's end on D_i . The centerlines of all the feasible tunnels constitute the goal region \mathcal{G} . We pick a constant number of equidistant goals on the line segment to plan for the manipulator (COMPUTETARGETPOSES method on line 6 in Algorithm 1). Our algorithm computes the paths from \mathbf{x}^S to cover \mathcal{G} by satisfying the goal criteria described above.

2) *Query Stage*: In the query stage, for a given query $g \in \mathcal{G}$, in the first step, the corresponding centerline is identified. This is done by first computing the points of intersection of the projectile on D_o and D_i and then finding the cells within which the points lie. In the second step, the associated path is retrieved from the lookup table constructed in the previous step. Specifically, for the initial estimate received by the planning module, we query the lookup table to obtain a manipulator trajectory from \mathbf{x}^S to g_1 . For all the remaining estimates, we use the tensor to check if a transition from g_i

to g_j is possible. If it is, then the corresponding trajectory is executed by the manipulator.

Algorithm 1 Generate Trajectory Database

```

1: Inputs: Motion planner  $\mathbf{P}$ , Home configuration  $\mathbf{x}^S$ ,
   Dome configuration  $\mathbf{C}$ 
2: Output: Trajectory database  $\mathbf{D}$ 
3: procedure PREPROCESS( $\mathbf{P}, \mathbf{x}^S, \mathbf{C}$ )
4:    $\mathbf{L} \leftarrow \text{COMPUTELINESEGMENTS}(\mathbf{C})$ 
5:   for  $l_i$  in  $\mathbf{L}$  do
6:      $\mathbf{T}_i \leftarrow \text{COMPUTETARGETPOSES}(l_i)$ 
7:      $\text{TrajBuffer} = []$ 
8:     for  $t$  in  $\mathbf{T}_i$  do
9:       if  $\text{IK}(\mathbf{x}^S, t)$  succeeds then
10:        if  $\mathbf{P}(\mathbf{x}^S, t)$  succeeds then
11:          Add resulting plan to  $\text{TrajBuffer}$ .
12:        end if
13:      end if
14:    end for
15:    Add least-time trajectory in  $\text{TrajBuffer}$  to  $\mathbf{D}$ .
16:  end for
17: end procedure

```

Algorithm 2 INSAT

```

1: procedure MAIN( $\mathbf{x}^S, \mathbf{x}^G$ )
2:    $\mathbf{x}_L^{\text{next}} = \mathbf{x}^S$ 
3:   while  $\phi_{\mathbf{x}^S \mathbf{x}^G}$  is EMPTY do
4:     Pick the next node  $\mathbf{x}_L^{\text{next}}$  to expand  $\triangleright$  Low-D graph
       search algorithm
5:     Generate the successors  $\mathbf{X}_L^{\text{new}}$  of  $\mathbf{x}_L^{\text{next}}$   $\triangleright$  Low-D
       graph search algorithm
6:     for  $\mathbf{x}_L^{\text{new}}$  in  $\mathbf{X}_L^{\text{new}}$  do
7:       Get the ancestors  $\mathbf{X}_L^{\text{pred}}$  of  $\mathbf{x}_L^{\text{new}}$ 
8:       for  $\mathbf{x}_L^{\text{pred}}$  in  $\mathbf{X}_L^{\text{pred}}$  do
9:          $\phi_{\mathbf{x}_L^{\text{pred}} \mathbf{x}_L^{\text{new}}} = \text{TRAJOPT}(\mathbf{x}_L^{\text{pred}}, \mathbf{x}_L^{\text{new}})$ 
10:        if  $\phi_{\mathbf{x}_L^{\text{pred}} \mathbf{x}_L^{\text{new}}}$  is VALID then
11:           $\phi_{\mathbf{x}^S \mathbf{x}_L^{\text{new}}} = \text{TRAJOPTWITHWARMSTART}(\phi_{\mathbf{x}^S \mathbf{x}_L^{\text{pred}}},$ 
              $\phi_{\mathbf{x}_L^{\text{pred}} \mathbf{x}_L^{\text{new}}})$ 
12:          if  $\phi_{\mathbf{x}^S \mathbf{x}_L^{\text{new}}}$  is VALID and  $c(\phi_{\mathbf{x}^S \mathbf{x}_L^{\text{new}}}) \leq c(\mathbf{x}_L^{\text{new}})$ 
             then
13:             $c(\mathbf{x}_L^{\text{new}}) = c(\phi_{\mathbf{x}^S \mathbf{x}_L^{\text{new}}})$ 
14:            Set  $\mathbf{x}_L^{\text{pred}}$  as the parent of  $\mathbf{x}_L^{\text{new}}$ 
15:            Store  $\phi_{\mathbf{x}^S \mathbf{x}_L^{\text{new}}}$ 
16:          return  $\phi_{\mathbf{x}^S \mathbf{x}^G}$ 
17:        end if
18:      end for
19:    end for

```

E. Kinodynamic Planning using INSAT

Kinodynamic planning is a class of problems for which velocity, acceleration, and inertial/force/torque bounds must be satisfied, together with kinematic constraints such as avoiding obstacles. However, controllers in fully actuated systems like the vast majority of commercial manipulators do not require a fully dynamically feasible trajectory to track them accurately. In such systems, even a velocity controller is able to track trajectories generated with smooth splines

[16] at high accuracy. As a result, planning in the space of the manipulator's joint space and its derivatives simplifies into finding the parameters of the choice of basis splines. This dramatic reduction in the planning complexity resulting from the spline representation of the manipulator trajectory enables us to use a recent global kinodynamic planning algorithm called INSAT [17] as the preprocessing planner. In this section, we will first explain our choice of splines and provide a high-level overview of INSAT. We refer the reader to [17], [18] for a details of the algorithm.

1) *B-Splines*: B-splines are smooth and continuous piecewise polynomial functions made of finitely many basis polynomials called B-spline bases. A k -th degree B-spline basis with m control points can be calculated using the Cox-de Boor recursion formula [19] as

$$N_{i,k}(t) = \frac{t - t_i}{t_{i+k-1} - t_i} N_{i,k-1}(t) + \frac{t_{i+k} - t}{t_{i+k} - t_{i+1}} N_{i+1,k-1}(t) \quad (2)$$

where $i = 0, \dots, m$, $\frac{t-t_i}{t_{i+k-1}-t_i}$ and $\frac{t_{i+k}-t}{t_{i+k}-t_{i+1}}$ are the interpolating coefficients between t_i and t_{i+k} . Let us define a non-decreasing knot vector \mathbf{T} and the set of control points $\mathbf{P} = \{\mathbf{p}_1, \mathbf{p}_2, \dots, \mathbf{p}_m\}$ where $\mathbf{p}_i \in \mathbb{R}^n, i = 0, \dots, m$. Then a B-spline trajectory can be uniquely determined by the degree of the polynomial k , the knot vector \mathbf{T} , and the set of control points \mathbf{P} called de Boor points.

$$\mathbf{q}(t) = \sum_{i=0}^m \mathbf{p}_i N_{i,k}(t) \quad (3)$$

The pseudocode of INSAT is given in Alg. 2. INSAT alternates between searching a low-D discrete graph and performing trajectory optimization in high-D to produce smooth full-D trajectories. The low-D variables in the algorithm are denoted with subscript L and the full-D trajectories connecting two lifted spaces of low-D state are \mathbf{x} and \mathbf{x}' is denoted as $\phi_{\mathbf{x}\mathbf{x}'}$. For the TRAJOPT step we solve the following optimization problem in Eq. 4 using the aforementioned B-spline representation.

$$\min \quad w_1 t_f + w_2 \int_0^{t_f} \|\dot{\mathbf{x}}(t)\|_2 dt \quad (4a)$$

$$\text{s.t.} \quad \mathbf{x} \in \mathcal{C}^n \quad (4b)$$

$$\mathbf{x}(t) \in \mathcal{X}^{free} \quad (4c)$$

$$\dot{\mathbf{x}}(t) \in [\dot{\mathbf{x}}_{min}, \dot{\mathbf{x}}_{max}] \quad (4d)$$

$$t_f \in [t_{min}, t_{max}] \quad (4e)$$

$$\mathbf{x}(t_0) = \mathbf{x}_0, \mathbf{x}(t_f) = \mathbf{x}_f \quad (4f)$$

$$\dot{\mathbf{x}}(t_0) = \dot{\mathbf{x}}_0, \dot{\mathbf{x}}(t_f) = \dot{\mathbf{x}}_f \quad (4g)$$

The optimization is performed over the control points of the B-splines. The precise details of the optimization are not mentioned here due to the page limit. Once the preprocessing module's request is received INSAT kicks to find a smooth B-spline from start to goal. When the output of the optimization is valid in terms of the dynamic limits but results in collision, we recover the trajectory by caching the iterates and return the last best trajectory to the preprocessor.

F. Perception Module

Predicting the trajectory of the incoming projectile is crucial for a successful intercept. This problem introduces two challenges:

- 1) A single stereo camera is placed on the 8020 aluminum T-slotted profiles, mounted on the robot arm's pedestal. Consequently, precise camera calibration is important to establish the extrinsic rigid body transformation between the camera frame and the robot's base frame.
- 2) The perception system should detect the rapidly moving projectile and provide an accurate projectile estimate of the projectile in real-time during its flight.

We solve the first challenge with hand-eye camera extrinsic calibration (IV-F.2) and solve the second challenge by performing a least-squares model fitting based on all observations (IV-F.3).

1) *Object Detection*: To detect the incoming projectile, we employ RGB color filtering since the projectile is characterized by its distinct color as a ball. We establish specific lower and upper color thresholds within the HSV color space, then process each frame to generate a binary mask that isolates the ball.

2) *Depth Estimation*: Masked point cloud information and confidence map are retrieved from the ZED SDK, with our Python API acting as a wrapper around the SDK.

We filter out outliers and eliminate point clouds falling outside the predefined virtual bounding box. To obtain the 3D global coordinates relative to the robot's base, we use "hand-eye" calibration techniques, facilitating the transformation between the left camera frame and the robot's base frame. Then, we compute the mean values for X , Y , and Z to derive the 3D centroid point. Frames that exceed a minimum pixel threshold are considered. Since depth data given by ZED is estimated, some depth points may not be entirely accurate. To address this, we implement depth confidence filtering, giving each pixel in the image a confidence value in the range of $[1, 100]$. Pixels with values close to 100 are deemed trustworthy. Consequently, we perform depth filtering, only retaining frames where the estimated depth falls within the specified distance threshold. Positions in these frames are recorded along with timestamps, and this iterative process continues until the required number of frames is collected.

3) *Projectile Estimation*: To reconstruct the 3D ball trajectory, we use the Ohno method [20]. Firstly, we fit multiple position detections at various time intervals to a projectile equation of motion. The motion is assumed to be on the $X-Z$ plane (with Z pointing vertically upwards). Movements perpendicular to this plane which can occur due to wind effects or other external forces are ignored. The ball motion is governed by gravity, which is expressed as

$$X(t) = X(0) + tV_X(0), \quad (5)$$

$$Y(t) = Y(0) + tV_Y(0), \quad (6)$$

$$Z(t) = Z(0) + tV_Z(0) - \frac{1}{2}gt^2. \quad (7)$$

where $(X(t), Y(t), Z(t))$ and $(V_X(t), V_Y(t), V_Z(t))$ denote the position and the velocity of the ball at time t , g denotes

the acceleration of gravity ($g = 9.81m/s^2$). Since the physical model is known, the estimated position at time t only depends on the initial position ($X(t), Y(t), Z(t)$) and the initial velocity ($V_X(t), V_Y(t), V_Z(t)$).

Secondly, we estimate the values of initial position and initial velocity $\theta = (X(0), Y(0), Z(0), V_X(t), V_Y(t), V_Z(t))$ by defining an error function that minimizes the sum of squared errors:

$$\theta^* = \arg \min_{\theta} \sum_{t=1}^M \{(X_t - X(t))^2 + (Y_t - Y(t))^2 + (Z_t - Z(t))^2\} \quad (8)$$

where $X(t), Y(t), Z(t)$ are the estimated positions from Eqn. 2–4 and X_t, Y_t, Z_t are observed positions from the detected frames in IV-F.2.

V. EXPERIMENTS AND RESULTS

A. Evaluation in Simulation

We evaluate the motion planning module first in simulation. The environment configuration in simulation is shown in Fig. 5, where the yellow cube outlines the inner dome and the red cube outlines the outer dome. A pink cylinder pole is added into the environment as an obstacle. We randomly sampled 400 projectiles for the experiment and verified that they intersect with the inner dome and outer dome. The launch distance for each projectile was uniformly sampled from a range of 6–12m. These projectiles have an average time of flight of 1.069s. Note that the time constraint is relaxed due to the addition of the obstacle, forcing the manipulator to take longer to execute a trajectory. All the experiments were carried out on an AMD Threadripper Pro 5995WX workstation. We compared our planning framework with two efficient online planners: the rapidly-exploring random tree connect (RRT-Connect) [21] and the edge-based parallel A* for slow evaluation (ePA*SE) [22]. The RRT-Connect is known to be efficient in solving single-query path planning problems, while ePA*SE is a recent work that leverages the power of parallelization to speed up the search. All online planners were given a 2-second budget to plan. The preprocessing time of our planning framework is 5 hours.

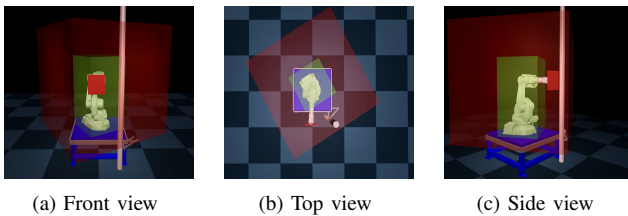


Fig. 5. (a), (b), and (c) are the front, top, and side views of the system in the Mujoco simulator.

The experimental results for 400 projectiles are shown in Table I. The first row is the ratio of the planner finding a solution to intercept the incoming projectile. The second row is the ratio of the successful blocking, meaning that the sum of the planning query time and the execution time is less than the time of flight of the incoming projectile. The

TABLE I
EVALUATING THE PLANNING MODULE IN SIMULATION

Metrics	Our approach	RRT-Connect	ePA*SE
Find Solution	72.75%	73.75%	49.75%
Success Rate	72.75%	27.75%	23.5%
Query Time (ms)	0.127 ± 0.0418	27.4 ± 41.1	268 ± 422
Execution Time (ms)	299 ± 119	1658 ± 1166	840 ± 362

third and fourth rows are the mean and the standard deviation of the planner query time and trajectory execution time in millisecond.

The experimental results demonstrate the superior performance of our method compared to the two baseline approaches. Specifically, our method achieves an exceptional success rate, nearly 3 times that of RRT-Connect and 3 times that of ePA*SE. In terms of the query time, our method is faster than RRT-Connect by a factor of 215 and ePA*SE by 2110, affirming our planner’s ability to swiftly compute manipulator trajectory paths within a short time window. Moreover, the execution time is substantially shorter than that of the two baseline approaches, further highlighting the efficiency of our methodology.

B. Experiments on Real Robot without Obstacles

We tested the full system with integrated perception on the ABB’s IRB-1600 robot arm and an onboard stereo camera ZED 2i in a basement environment. We set up the range of attacks to be 6–8m. In this setting, the time of flight of the ball from its first detection by the perception system to its interception with the robot is roughly 350ms. Out of which, on average, 82.9ms is used by the perception system, 212.2ms is the trajectory execution time for the robot and 50ms is taken up by other system overheads. That leaves only 4.9ms for the planner on average. Our planner successfully generates a plan within this time budget.

We performed 50 throws and achieved a blocking success rate of 78%. Among the 11 throws that were unsuccessful, the causes of these failures were traced back to issues within the perception and execution modules. Specifically, in 8 instances, inaccuracies in the perception module arose due to motion blur or noisy depth estimations. The remaining three failures were attributed to slow execution processes. This occurred when the execution time for specific trajectories either outpaced the perception module’s ability to provide timely updates or when executing the entire trajectory consumed more time than the actual time of flight of the ball.

VI. CONCLUSION AND FUTURE WORK

In this paper, we have presented and evaluated a preprocessed kinodynamic motion planning framework for intercepting projectiles using a robot manipulator. We tested our overall pipeline which consists of a perception module, a planner module, and an execution module on a real-world robotic system. In the future, we would like to extend this work to a mobile base and intercept multiple projectiles.

REFERENCES

- [1] J. Tebbe, L. Klamt, Y. Gao, and A. Zell, “Spin detection in robotic table tennis,” in *2020 IEEE international conference on robotics and automation (ICRA)*, pp. 9694–9700, IEEE, 2020.

- [2] P. Cigliano, V. Lippiello, F. Ruggiero, and B. Siciliano, "Robotic ball catching with an eye-in-hand single-camera system," *IEEE Transactions on Control Systems Technology*, vol. 23, no. 5, pp. 1657–1671, 2015.
- [3] B. Büml, T. Wimböck, and G. Hirzinger, "Kinematically optimal catching a flying ball with a hand-arm-system," in *2010 IEEE/RSJ International Conference on Intelligent Robots and Systems*, pp. 2592–2599, 2010.
- [4] D. Büchler, S. Guist, R. Calandra, V. Berenz, B. Schölkopf, and J. Peters, "Learning to play table tennis from scratch using muscular robots," *arXiv preprint arXiv:2006.05935*, 2020.
- [5] K. Mülling, J. Kober, O. Kroemer, and J. Peters, "Learning to select and generalize striking movements in robot table tennis," *The International Journal of Robotics Research*, vol. 32, no. 3, pp. 263–279, 2013.
- [6] S. M. Kakade, *On the sample complexity of reinforcement learning*. University of London, University College London (United Kingdom), 2003.
- [7] A. Agarwal, Y. Han, and M. Likhachev, "Perch 2.0: Fast and accurate gpu-based perception via search for object pose estimation," in *2020 IEEE/RSJ International Conference on Intelligent Robots and Systems (IROS)*, pp. 10633–10640, IEEE, 2020.
- [8] R. A. Kromer, A. Abellán, D. J. Hutchinson, M. Lato, T. Edwards, and M. Jaboyedoff, "A 4d filtering and calibration technique for small-scale point cloud change detection with a terrestrial laser scanner," *Remote Sensing*, vol. 7, no. 10, pp. 13029–13052, 2015.
- [9] A. Pfister, A. M. West, S. Bronner, and J. A. Noah, "Comparative abilities of microsoft kinect and vicon 3d motion capture for gait analysis," *Journal of medical engineering & technology*, vol. 38, no. 5, pp. 274–280, 2014.
- [10] D. M. Ramík, C. Sabourin, R. Moreno, and K. Madani, "A machine learning based intelligent vision system for autonomous object detection and recognition," *Applied intelligence*, vol. 40, no. 2, pp. 358–375, 2014.
- [11] J. Redmon, S. Divvala, R. Girshick, and A. Farhadi, "You only look once: Unified, real-time object detection," in *Proceedings of the IEEE conference on computer vision and pattern recognition*, pp. 779–788, 2016.
- [12] F. Islam, O. Salzman, A. Agarwal, and M. Likhachev, "Provably constant-time planning and replanning for real-time grasping objects off a conveyor belt," *The International Journal of Robotics Research*, vol. 0, no. 0, p. 02783649211027194, 0.
- [13] M. Likhachev, G. J. Gordon, and S. Thrun, "Ara*: Anytime a* with provable bounds on sub-optimality," *Advances in neural information processing systems*, vol. 16, 2003.
- [14] M. Likhachev and D. Ferguson, "Planning long dynamically feasible maneuvers for autonomous vehicles," *The International Journal of Robotics Research*, vol. 28, no. 8, pp. 933–945, 2009.
- [15] I. Pohl, "Heuristic search viewed as path finding in a graph," *Artificial intelligence*, vol. 1, no. 3-4, pp. 193–204, 1970.
- [16] D. Constantinescu and E. A. Croft, "Smooth and time-optimal trajectory planning for industrial manipulators along specified paths," *Journal of robotic systems*, vol. 17, no. 5, pp. 233–249, 2000.
- [17] R. Natarajan, H. Choset, and M. Likhachev, "Interleaving graph search and trajectory optimization for aggressive quadrotor flight," *IEEE Robotics and Automation Letters*, vol. 6, no. 3, pp. 5357–5364, 2021.
- [18] R. Natarajan, G. L. H. Johnston, N. Simaan, M. Likhachev, and H. Choset, "Torque-limited manipulation planning through contact by interleaving graph search and trajectory optimization," 2022.
- [19] N. M. Patrikalakis, "Approximate conversion of rational splines," *Computer Aided Geometric Design*, vol. 6, no. 2, pp. 155–165, 1989.
- [20] Y. Ohno, J. Miura, and Y. Shirai, "Tracking players and estimation of the 3d position of a ball in soccer games," *Proceedings 15th International Conference on Pattern Recognition. ICPR-2000*, vol. 1, pp. 145–148 vol.1, 2000.
- [21] J. J. Kuffner and S. M. LaValle, "Rrt-connect: An efficient approach to single-query path planning," in *Proceedings 2000 ICRA. Millennium Conference. IEEE International Conference on Robotics and Automation. Symposia Proceedings (Cat. No. 00CH37065)*, vol. 2, pp. 995–1001, IEEE, 2000.
- [22] S. Mukherjee, S. Aine, and M. Likhachev, "epa* se: Edge-based parallel a* for slow evaluations," in *Proceedings of the International Symposium on Combinatorial Search*, vol. 15, pp. 136–144, 2022.